Journal of Biomedical Optics

SPIEDigitalLibrary.org/jbo

Three-dimensional computational analysis of optical coherence tomography images for the detection of soft tissue sarcomas

Shang Wang
Chih-Hao Liu
Valery P. Zakharov
Alexander J. Lazar
Raphael E. Pollock
Kirill V. Larin

SPIE

Three-dimensional computational analysis of optical coherence tomography images for the detection of soft tissue sarcomas

Shang Wang,[a] Chih-Hao Liu,[a] Valery P. Zakharov,[b] Alexander J. Lazar,[c] Raphael E. Pollock,[c] and Kirill V. Larin[a,d]
[a]University of Houston, Department of Biomedical Engineering, 3605 Cullen Boulevard, Houston, Texas 77204-5060
[b]Samara State Aerospace University, Department of Radiotechnical Engineering, Moskovskoe shosse 34, Samara, 443086, Russia
[c]The University of Texas M.D. Anderson Cancer Center, Sarcoma Research Center, 1515 Holcombe Boulevard, Houston, Texas 77030
[d]Baylor College of Medicine, Department of Molecular Physiology and Biophysics, One Baylor Plaza, Houston, Texas 77030

Abstract. We present a three-dimensional (3-D) computational method to detect soft tissue sarcomas with the goal of automatic surgical margin assessment based on optical coherence tomography (OCT) images. Three parameters are investigated and quantified from OCT images as the indicators for the tissue diagnosis including the signal attenuation (A-line slope), the standard deviation of the signal fluctuations (speckles), and the exponential decay coefficient of its spatial frequency spectrum. The detection of soft tissue sarcomas relies on the combination of these three parameters, which are related to the optical attenuation characteristics and the structural features of the tissue. Pilot experiments were performed on *ex vivo* human tissue samples with homogeneous pieces (both normal and abnormal) and tumor margins. Our results demonstrate the feasibility of this computational method in the differentiation of soft tissue sarcomas from normal tissues. The features of A-line-based detection and 3-D quantitative analysis yield promise for a computer-aided technique capable of accurately and automatically identifying resection margins of soft tissue sarcomas during surgical treatment. [DOI: 10.1117/1.JBO.19.2.021102]

Keywords: optical coherence tomography; soft tissue sarcomas; computational image analysis.

Paper 130207SSR received Apr. 2, 2013; revised manuscript received Apr. 29, 2013; accepted for publication May 1, 2013; published online Jun. 27, 2013.

1 Introduction

Soft tissue sarcomas develop within connective tissues such as fibrous tissue, fat, and muscle.[1,2] Surgical resection is currently the most effective treatment for the patients with this disease.[3] However, the macroscopic resemblance between the pathological and normal soft tissues causes it difficult to delineate the negative tumor resection margins intraoperatively, as one of the key reasons that result in high local recurrence rate of soft tissue sarcomas.[4] Currently, tissue biopsy is the only clinical method for tumor detection, but its requirement of tissue sampling limits the accuracy of assessment and leads to significant delay in completing the surgical resection. [5] Thus, enhanced surgical techniques based on real-time microscopic imaging and detection is required to reduce the chance of local recurrence, minimize the resection region, and improve the efficiency of surgical treatment of soft tissue sarcomas.

Optical coherence tomography (OCT) is a noninvasive imaging technique with high spatial and temporal resolutions.[6,7] The typical imaging depth of OCT can reach 1 to 3 mm in most highly scattering tissues.[8] OCT-based tumor detection methods have been developed mainly based on the imaging of tissue structures,[9–12] the assessment of tissue optical properties,[13–15] and the measurement of tissue elasticity.[16,17] For the imaging-guided detection of soft tissue sarcomas with OCT, recent study by Carbajal et al. has demonstrated that the morphology of liposarcoma and normal adipose tissue can be distinguished based on the OCT images, suggesting the possibility of using OCT for the surgical identification of soft tissue sarcomas.[18] However, to meet the requirement of clinical use, there must be certain effective indicators for the diagnosis of soft tissue sarcomas through the computational analysis of OCT images that could aid surgeons with their decision process. As the use of OCT for the detection of breast cancer and oral cancer,[19,20] computational methods are expected to offer assistance in the transition to clinical applications.

In this paper, we present a three-dimensional (3-D) computational method to analyze the OCT images for the detection of soft tissue sarcomas. Three effective indicators, including the signal attenuation as a function of depth (A-line slope), the standard deviation of the signal fluctuations of slope-removed A-line, and the exponential decay coefficient of its spatial frequency spectrum, are combined to provide an advanced diagnosis of the tissue types. The differentiation is based on the quantitative analysis of the optical attenuation property and the structure information of the tissues. Our results suggest this method can be potentially utilized as a computer-aided high-resolution automatic identification technique for the surgical resection of soft tissue sarcomas.

2 Materials and Methods

2.1 *Swept-Source OCT System*

We utilized a home-built swept-source OCT system to image the soft tissue samples. The details of the system description are

Address all correspondence to: Kirill V. Larin, University of Houston, Department of Biomedical Engineering, 3605 Cullen Boulevard, Houston, Texas 77204-5060. Tel: 832-842-8834; Fax: 713-743-0226; E-mail: klarin@uh.edu

0091-3286/2014/$25.00

presented in our previous work.[21,22] Briefly, the system utilized a swept laser source (Santec, Inc., Komaki, Aichi, Japan) which has a central wavelength of 1310 nm with a bandwidth of ~150 nm. The scanning rate over full operating wavelength is 30 kHz, which determines the system temporal resolution of ~33 μs. The OCT system is based on a Mach–Zehnder interferometer, where the light from the reference and the sample arms interference. The fringes are recorded through a balanced photodetector, and the signal is digitized by a high-speed analog to digital convertor (Alazar Tech, Inc., Quebec, Canada). Fast Fourier transform is applied to the k-equally spaced interference signals, and the resulted intensity A-lines are presented with dB unit. Depth-resolved two-dimensional (2-D) images of tissue samples can be real-time visualized from the computer. The system can provide an axial resolution of ~15 μm and an imaging depth of ~9 mm (both in air). The transverse resolution of the system is around 15 μm, and the sensitivity is up to 100 dB. During OCT imaging, the focal plane of scan lens was kept at the surface position of the tissue samples for minimizing the effect of the focal function on the computational analysis.

2.2 *Soft Tissue Samples*

For the demonstration of our method, pilot experiments were performed on *ex vivo* human tissues with two types of samples: homogeneous pieces (both normal and abnormal) and tumor margin. For the former, fat, skeletal muscle, well-differentiated liposarcoma (WDLS), and leiomyosarcoma were used in the experiments, and total six pieces of samples from six patients were involved. WDLS is one type of liposarcoma that develops in the tissue of fat, and leiomyosarcoma is a cancer of smooth muscle. For the latter, we conducted our feasibility study on the tissue with the interface between collagen, a normal type of fibrous tissue, and cellular fibrous tumor. All tissue samples were taken from the surgical resection at the University of Texas M.D. Anderson Cancer Center (UTMADCC) Hospital. Sterile phosphate buffered saline was used to keep the samples until the experiments. OCT imaging was performed within 12 h after the surgical resection. The protocols of tissue processing were approved by the UTMDACC and the University of Houston Biosafety Committees. After the experiments, the tissue samples were fixed with formalin, and the hematoxylin and eosin (H&E) stained histology analysis was performed. A UTMADCC sarcoma pathologist conducted the diagnosis and the classification of the samples.

2.3 *Computational Method*

The computational analysis is based on individual A-line (with dB unit in log scale) from OCT images. The whole procedure is presented in Fig. 1 with a typical A-line from the OCT imaging of human leiomyosarcoma. Due to the large refractive index change at the air–tissue interface, high reflections of light usually occur at the surface of tissue samples, which can result in relatively large intensity jumps, as shown in Fig. 1(a). To avoid the influence of this effect on the computations, we choose the start of the target region ~40 μm below the tissue surface. As illustrated in Fig. 1(a), an axial region of ~0.7 mm is selected for the A-line processing. The selection of this ~0.7 mm depth region is based on our purpose of including as much depth information as possible from the OCT images for computation, and at the same time keeping the size of the depth region constant over the processing for all types of soft tissues. For each extracted A-line, a linear fit is applied to the signal, and the slope value is achieved as the first parameter to characterize the tissue, as shown in Fig. 1(b). Then, the slope information from the A-line is removed by performing a subtraction of the linear fitting function, and thus, resulting in an intensity signal with the mean of approximately zero, as shown in Fig. 1(c). The standard deviation of the intensity signal is calculated as the second parameter for tissue differentiation. A fast Fourier transform is then applied on this intensity signal, and the amplitude information of the spatial frequency spectrum is utilized for an exponential fit with the function of $y = Ae^{-Bx}$, as shown in Fig. 1(d). The exponential decay coefficient B is obtained as the third parameter for the characterization of tissue. The A-line slope, the standard deviation of slope-removed A-line, and the exponential decay coefficient of its spatial frequency spectrum are finally presented as the indicators of the soft tissue types and are combined together for advanced tissue diagnosis with 3-D information.

In soft tissues, the intensity of transmitted light, I, can be first-order approximated by the Beer–Lambert law, $I = I_0 e^{-\mu z}$, where μ is the attenuation coefficient of light, I_0 is the incident light intensity, and z is the depth of light traveling inside the tissue.[23] Thus, with the intensity values rescaled in dB unit, the measured slope value is determined by the optical attenuation property of the soft tissue for which a higher slope indicates a larger optical attenuation coefficient of the tissue sample. As OCT detects the backscattered light from the tissue, the mismatch of the refractive index inside the tissue provides the contrast of OCT depth-resolved images.[24] With the slope removed, the OCT A-line signal can be a representation of the variations of tissue refractive index (structure) along the depth. Hence, the amplitude and frequency of the intensity fluctuation, characterized by the standard deviation of the slope-removed A-line and the exponential decay coefficient of its spatial frequency spectrum, respectively, are dependent on the structural features of the soft tissues. Specifically, a greater variation of refractive index along the depth will result in a higher value of standard deviation; also, a larger exponential decay coefficient suggests that there exist more of low frequency components in the change of tissue refractive index. Therefore, the combination of these three parameters provides relatively thorough characteristics of the tissue samples.

3 Results

3.1 *Homogeneous Fat and WDLS*

Figure 2 shows the selected H&E histology images [Fig. 2(a) and 2(d)] for fat and WDLS with the corresponding depth-resolved 2-D OCT images [Fig. 2(b) and 2(e)] and typical A-lines [Fig. 2(c) and 2(f)], respectively. By comparing with the histology results, it can be seen that OCT images clearly reveal the morphology of the tissues of fat and WDLS. Specifically, the adipocytes can be easily distinguished with the cell shape presented in OCT images. An important feature can be seen from the OCT images that WDLS involves more nonadipocyte-structure areas compared with fat, which can be explained by the presence of thicker septa in WDLS.[25] From the typical A-lines, it is clear that over the 1.8 mm depth differences exist between the fat and WDLS in terms of the slope of the signal and the amplitude and frequency of the intensity fluctuation.

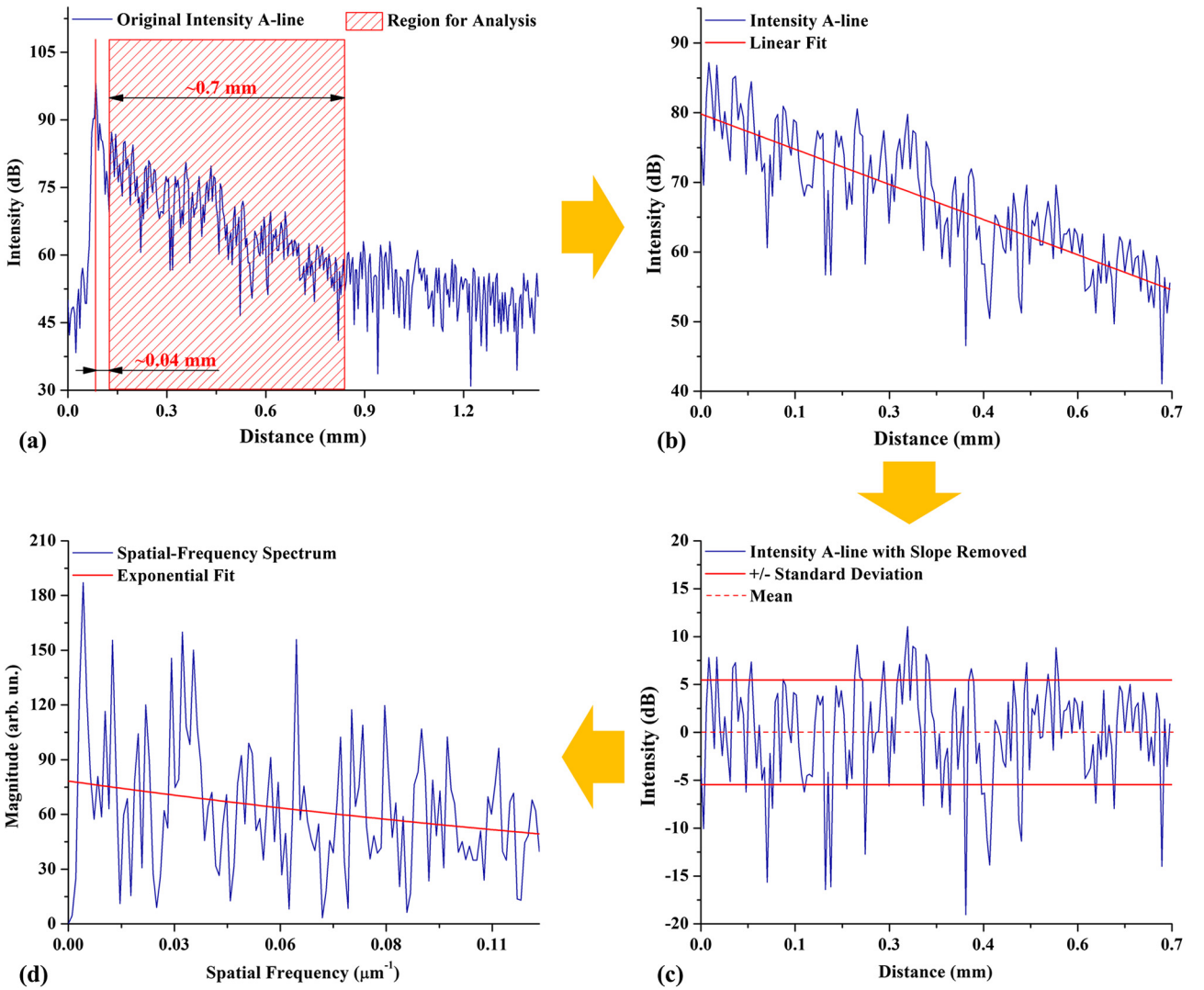

Fig. 1 Computational procedure illustrated with A-line from the optical coherence tomography (OCT) imaging of human leiomyosarcoma. (a) Original intensity A-line with the indication of the region for analysis; (b) indication of linear fit of A-line for the slope value; (c) slope-removed A-line for the standard deviation calculation; (d) spatial frequency spectrum presented with the amplitude information for exponential fit to quantify the exponential decay coefficient.

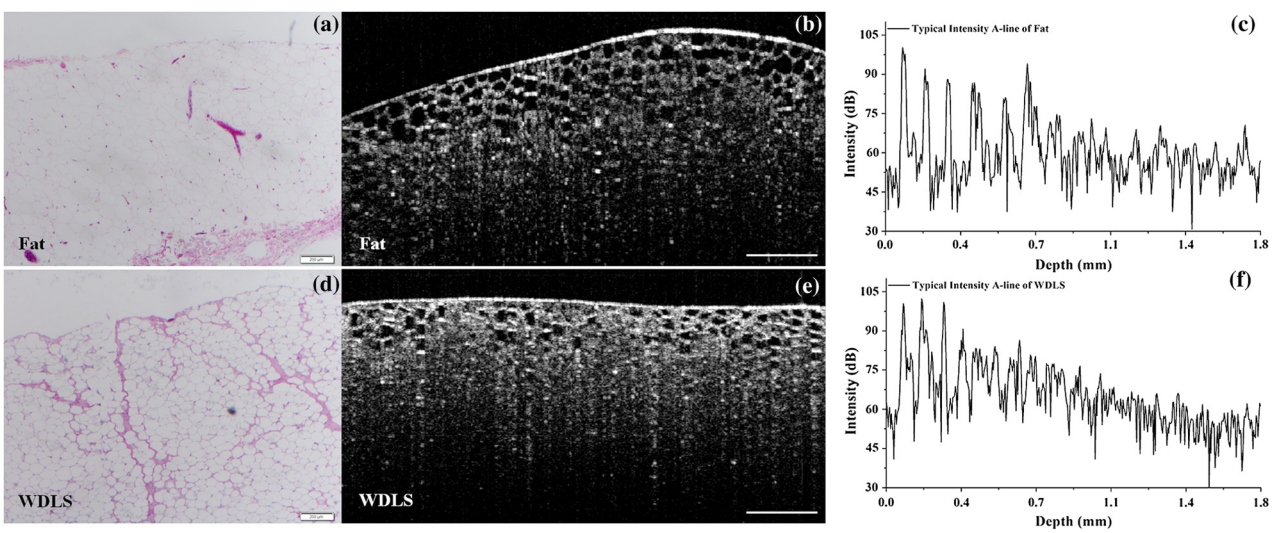

Fig. 2 Selected histology images (a) and (d) for fat and well-differentiated liposarcoma (WDLS), respectively; corresponding OCT images (b) and (e) for fat and WDLS, respectively; typical A-lines (c) and (f) from OCT images of fat and WDLS, respectively. The scale bars in (b) and (e) represent 0.5 mm.

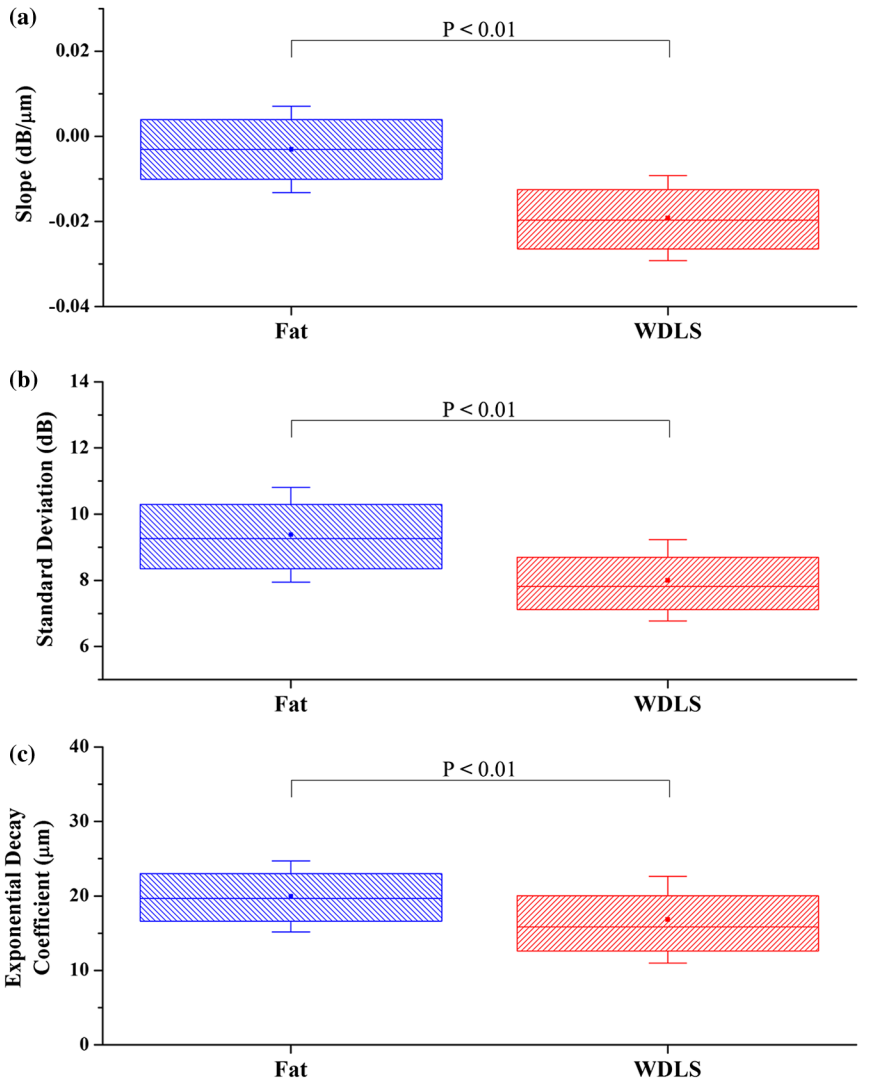

Fig. 3 Box plots of the quantified results of (a) the A-line slope, (b) the standard deviation of the slope-removed A-line, and (c) the exponential decay coefficient of the spatial frequency spectrum of slope-removed A-line for fat and WDLS. The solid dots and the whiskers represent the mean and the standard deviation of the data, respectively. $N = 40{,}000$ and 240,000 for the measurements conducted on the tissues of fat and WDLS, respectively. The P values are from the two-sample unequal-variance Student's t-tests.

The quantitative representations of these differences are presented in Fig. 3, which shows the statistical results of fat and WDLS with the parameters of the A-line slope, the standard deviation of the slope-removed A-line, and the exponential decay coefficient of its spatial frequency spectrum. Data points from 40,000 and 240,000 recording positions are involved for fat and WDLS, respectively. The slope values of A-line are quantified as -0.0031 ± 0.0102 dB/μm for fat and -0.0192 ± 0.0100 dB/μm for WDLS, as shown in Fig. 3(a). The higher absolute value of the slope from WDLS indicates the tissue of WDLS, compared with fat, attenuates more of the laser light with the same penetration of depth. From Fig. 3(b), the computation of the standard deviation shows 9.4 ± 1.4 dB for fat and 8.0 ± 1.2 dB for WDLS, which indicates that there exist larger variation of refractive index along the depth in the tissue of fat. We also quantified the exponential decay coefficient of 19.9 ± 4.8 and 16.8 ± 5.8 μm for fat and WDLS, respectively, as shown in Fig. 3(c). This suggests that, relative to WDLS, in the tissue of fat more low frequency components exist in the depthwise change of refractive index. For each of the parameters, we performed two-sample unequal-variance Student's t-test and the results indicate all these three parameters can be effective indicators for the differentiation of WDLS from fat.

The combination of the three parameters provides the identification of WDLS and fat in a 3-D space of slope versus standard deviation versus exponential decay coefficient, as shown in Fig. 4. Figure 4(a) indicates the spatial regions occupied by these two types of tissues through the plots of the data points and the 95% confidence ellipsoids. The 2-D projections of the plots are shown in Fig. 4(b)–4(d). Based on the 3-D information, the tissues of WDLS and fat can be clearly distinguished.

3.2 *Homogeneous Skeletal Muscle and Leiomyosarcoma*

For the tissues of skeletal muscle and leiomyosarcoma, Fig. 5 shows the histology images [Fig. 5(a) and 5(d)], the corresponding OCT images [Fig. 5(b) and 5(e)], and typical A-lines [Fig. 5(c) and 5(f)], respectively. Based on the structural OCT images, the skeletal muscle and the leiomyosarcoma appear similar, because at the scale-level of the system spatial resolution the

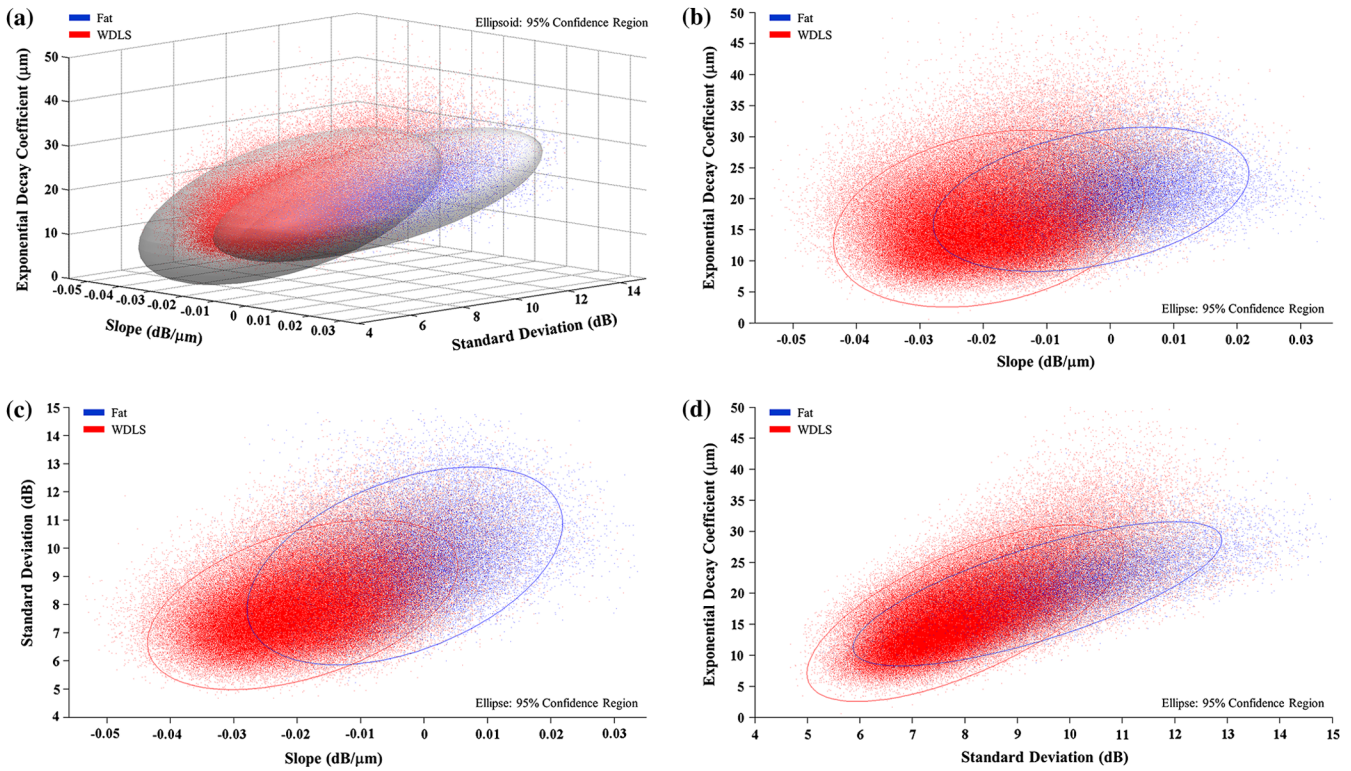

Fig. 4 (a) Three-dimensional (3-D) plot of the data points and the confidence ellipsoids (95%) for fat and WDLS in the spatial region composited by the parameters of the A-line slope, the standard deviation of the slope-removed A-line, and the exponential decay coefficient of its spatial frequency spectrum. Two-dimensional (2-D) projections are presented in the spatial plane of (b) exponential decay coefficient versus slope, (c) standard deviation versus slope, and (d) exponential decay coefficient versus standard deviation. $N = 40{,}000$ and 240,000 for the data points involved for fat and WDLS, respectively.

cells inside both types of the tissues are relatively homogeneous. However, from the intensity A-lines, differences can be clearly observed in the amplitude and frequency of the fluctuation of intensity as well as in the slope of the A-lines.

Similar to Fig. 3, for quantifying the differences between skeletal muscle and leiomyosarcoma, we present the statistical results of the A-line slope, the standard deviation of the slope-removed A-line, and the exponential decay coefficient of its spatial frequency spectrum in Fig. 6. Our computations involve a total of 40,000 and 80,000 data points from different measurement positions on the tissues of skeletal muscle and leiomyosarcoma, respectively. From Fig. 6(a), the skeletal muscle has a slope value of -0.0285 ± 0.0089 dB/μm, while the slope value for leiomyosarcoma is -0.0351 ± 0.0073 dB/μm. This

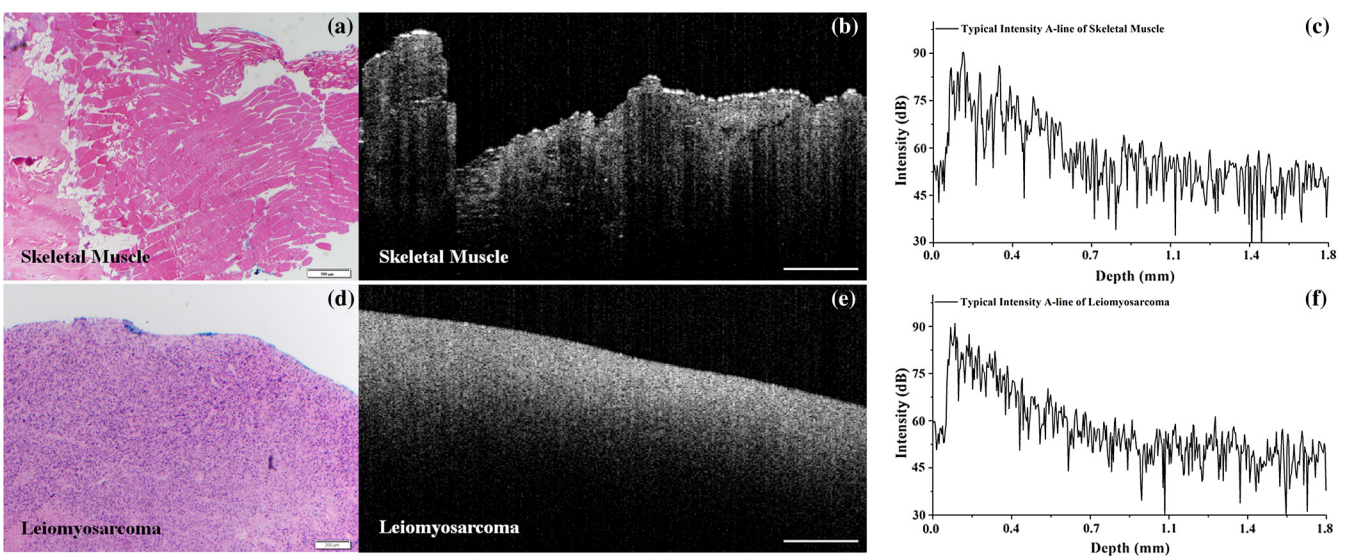

Fig. 5 Selected histology images (a) and (d) for skeletal muscle and leiomyosarcoma, respectively; corresponding OCT images (b) and (e) for skeletal muscle and leiomyosarcoma, respectively; typical A-lines (c) and (f) from OCT images of skeletal muscle and leiomyosarcoma, respectively. The scale bars in (b) and (e) represent 0.5 mm.

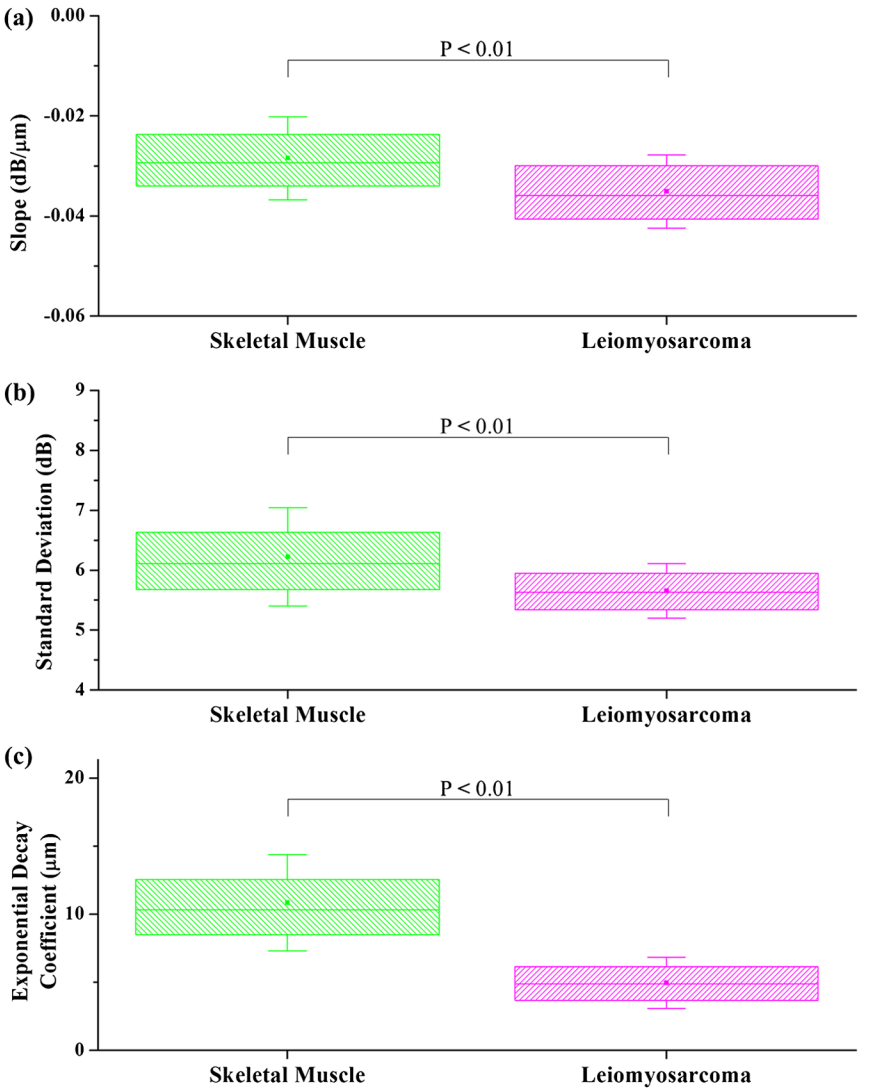

Fig. 6 Box plots of the quantified results of (a) the A-line slope, (b) the standard deviation of the slope-removed A-line, and (c) the exponential decay coefficient of the spatial frequency spectrum of slope-removed A-line for skeletal muscle and leiomyosarcoma. The solid dots and the whiskers represent the mean and the standard deviation of the data, respectively. $N = 40{,}000$ and 80,000 for the measurements conducted on the tissues of skeletal muscle and leiomyosarcoma, respectively. The P values are from the two-sample unequal-variance Student's t-tests.

difference indicates, with respect to the wavelength range from the laser source, the tissue of leiomyosarcoma has a relatively higher optical attenuation coefficient compared with skeletal muscle. In Fig. 6(b), our computations show a larger standard deviation of 6.2 ± 0.8 dB for skeletal muscle than 5.7 ± 0.5 dB for leiomyosarcoma, which suggests the variation of refractive index along the depth appears to be relatively lower in the tissue of leiomyosarcoma. Also, the exponential decay coefficients are quantified as 10.8 ± 3.5 μm for skeletal muscle and 4.9 ± 1.9 μm for leiomyosarcoma, as shown in Fig. 6(c). Compared with skeletal muscle, the lower value of exponential decay coefficient indicates that for the tissue of leiomyosarcoma, there are fewer of low frequency components existing in the refractive index change over depth. Similar to the study with fat and WDLS, we conducted the two-sample unequal-variance Student's t-test for all three parameters, and the differences between skeletal muscle and leiomyosarcoma have been found to be statistically significant.

The 3-D plots of the data points and the 95% confidence ellipsoids are presented in Fig. 7(a) indicating the relative positions of skeletal muscle and leiomyosarcoma in the spatial region composited by the three parameters. Figure 7(b)–7(d) show the corresponding 2-D projections for both the types of tissues. It can be clearly seen that the differentiation of leiomyosarcoma from the tissue of skeletal muscle can be achieved based on our 3-D computational method.

3.3 *Cellular Fibrous Tumor Margin with Collagen*

Our method is also demonstrated on the soft tissue sample with tumor margin. The histology result and the corresponding OCT image from the same location of the tissue are shown in Fig. 8(a) and 8(b), respectively. The vertical margin between the tissues of collagen and cellular fibrous tumor can be clearly visualized from the histology image. The 3-D computational method was performed for every individual A-line from the OCT image, and the quantified values are color-coded and plotted below the OCT image at the corresponding A-line positions. The color of red, green, and yellow are utilized to represent the parameters of the A-line slope, the standard deviation of the slope-removed

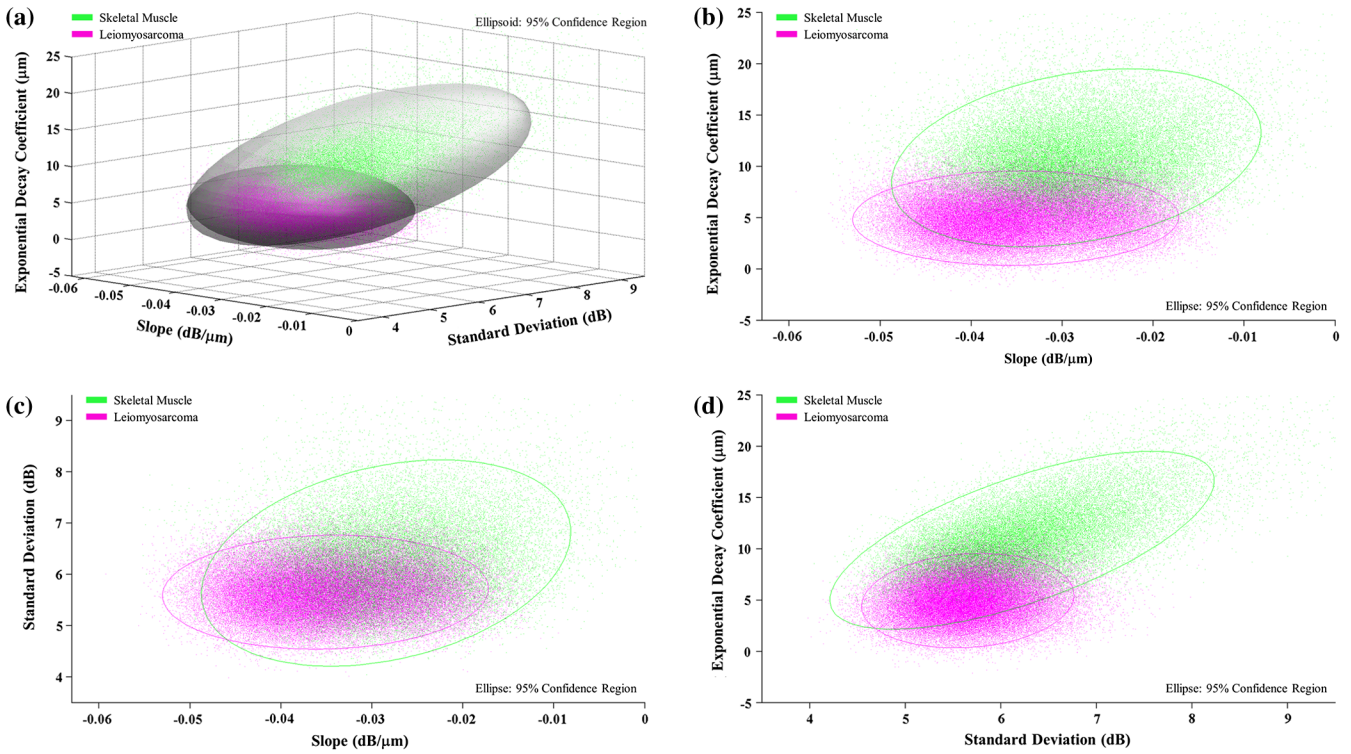

Fig. 7 (a) 3-D plot of the data points and the confidence ellipsoids (95%) for skeletal muscle and leiomyosarcoma in the spatial region composited by the parameters of the A-line slope, the standard deviation of the slope-removed A-line, and the exponential decay coefficient of its spatial frequency spectrum. 2-D projections are presented in the spatial plane of (b) exponential decay coefficient versus slope, (c) standard deviation versus slope, and (d) exponential decay coefficient versus standard deviation. $N = 40{,}000$ and 80,000 for the data points involved for skeletal muscle and leiomyosarcoma, respectively.

A-line, and the exponential decay coefficient of its spatial frequency spectrum, respectively. For all of them, darker regions represent larger values, while brighter regions indicate smaller values. Figure 8(c) is the combination of the three parameters with the overlap of three colors. It can be seen that the part of cellular fibrous tumor is relevant to the brighter regions of all three colors, suggesting the tissue of cellular fibrous tumor has higher attenuation of the light from the system laser, smaller variation of the refractive index and fewer of low frequency components for the refractive index change inside the tissue. The estimated position of the vertical tumor margin based on the 3-D computational method is indicated with blue arrows in Fig. 8. The good agreement with the histology results demonstrates the feasibility of our method in the accurate delineation of the vertical margin between cellular fibrous tumors and the tissue of collagen.

4 Discussions

These pilot studies demonstrate the feasibility of the proposed method in the detection of soft tissue sarcomas based on the

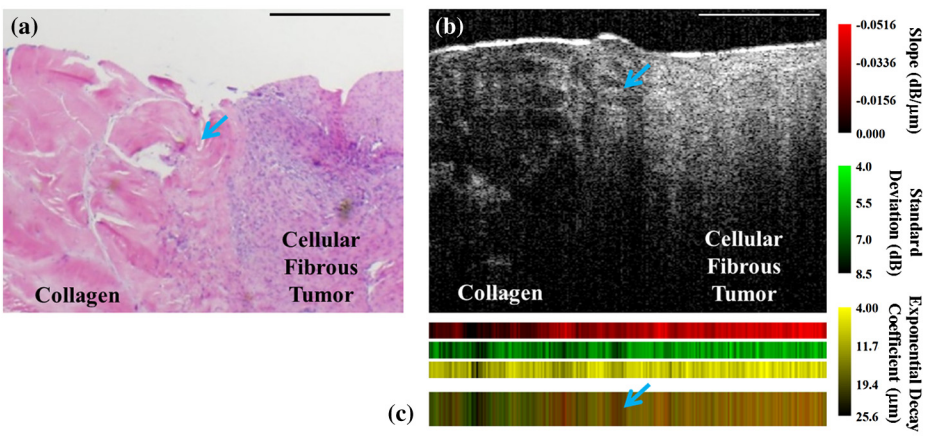

Fig. 8 Vertical tumor margin between collagen and cellular fibrous tumor presented with (a) histology image, (b) OCT image, and (c) color-coded plot combining the parameters of the A-line slope, the standard deviation of the slope-removed A-line, and the exponential decay coefficient of its spatial frequency spectrum. The arrows point at the estimated position of the vertical tumor margin. The scale bars represent 0.5 mm.

information of tissue optical property and structural features. We have found that the pathological tissues of WDLS, leiomyosarcoma, and cellular fibrous tumor appear to have smaller values of all three indicators compared with their corresponding normal tissue types. With the relationship of the parameters to the tissue characteristics, the results indicate that the optical attenuation coefficients of the three types of soft tissue sarcomas are higher than the relevant healthy types of tissues, and this effect turns out to be similar to the results observed in the breast cancer.[13,26] Also, in terms of the tissue structure, all the three pathological tissue types have shown reduced variation of tissue refractive index and fewer components of low frequency in the depthwise refractive index change. For the pair of WDLS and fat, this is caused by the thicker septa presented in the tissue of WDLS,[25] which compared with adipocytes, appears in the A-lines with smaller amplitude but higher frequency of intensity fluctuation. For the other two pairs of tissue types, the differences can be explained by the more compact cellular arrangement in the tissues of leiomyosarcoma and cellular fibrous tumor,[27,28] which can also be observed in Figs. 5(d) and 8(a).

Three features of the proposed method can be summarized as A-line-based computation, 3-D analysis, and quantitative detection. First, the computation of the individual A-line allows the method to achieve the same transverse spatial resolution of the OCT system. For the axial direction, the detection can also be performed for layered tissues with horizontal tumor margins by using a window of particular size to move and select regions for processing along the depth. However, in this case, the limited imaging depth of OCT technique may affect the areas inside the tissue that can be assessed. OCT system combined with forward or sideward scanning needle probe[29,30] can be considered to be incorporated with our method to address this problem. Second, the development of 3-D analysis is for including more thorough information from the tissues to assist the diagnosis of the tissue types. With the 3-D plot, training data can be presented with particular spatial reference regions, and this will provide a convenient visualization of the relative position where the testing data fall, which is expected to lead to a rapid assessment. Finally, the quantifications of the effective indicators provide more reliable information compared with the methods only based on the observation of the structural OCT images. Also, the quantitative detection holds the potential to be further developed into a computer-aided automatic detection technique.

As a feasibility study of the proposed method, the presented results provide the demonstration for the detection of WDLS and leiomyosarcoma and the delineation of the vertical margin of cellular fibrous tumor. To further investigate the efficiency of this method, more number of tissue samples should be included, full statistical analysis, including sensitivity and specificity, must be conducted, and the detection of other types of soft tissue sarcomas needs to be studied. The complete evaluation of this 3-D computational method will be the focus of our future work.

5 Conclusions

We have demonstrated a 3-D computational method to analyze OCT images for the detection of soft tissue sarcomas. Our method is based on the information of the tissue optical attenuation property and the structural features. Three effective indicators, including the A-line slope, the standard deviation of the slope-removed A-line, and the exponential decay coefficient of its spatial frequency spectrum, are presented and studied. The combination of these three parameters from OCT images offers advanced diagnosis of soft tissue types with the 3-D plots of data points and confidence ellipsoids in the spatial region composited by the parameters. With further evaluation, this method can be potentially developed as a computer-aided technique capable of accurately and automatically identifying resection margins of soft tissue sarcomas during surgical treatment.

Acknowledgments

This research is supported in part by the Federal Target Program "Scientific and scientific-pedagogic staff of innovative Russia in 2007–2013."

References

1. J. N. Cormier and R. E. Pollock, "Soft tissue sarcomas," *CA Cancer J. Clin.* **54**(2), 94–109 (2004).
2. R. E. Pollock, *American Cancer Society Atlas of Clinical Oncology: Soft Tissue Sarcomas*, BC Decker, Hamilton (2002).
3. R. E. Pollock et al., "The National Cancer Data Base report on soft tissue sarcoma," *Cancer* **78**(10), 2247–2257 (1996).
4. K. K. Tanabe et al., "Influence of surgical margins on outcome in patients with preoperatively irradiated extremity soft tissue sarcomas," *Cancer* **73**(6), 1652–1659 (1994).
5. M. H. G. Katz, E. A. Choi, and R. E. Pollock, "Current concepts in multimodality therapy for retroperitoneal sarcoma," *Expert Rev. Anticancer Ther.* **7**(2), 159–168 (2007).
6. M. E. Brezinski and J. G. Fujimoto, "Optical coherence tomography: high-resolution imaging in nontransparent tissue," *IEEE J. Sel. Top. Quant. Electron.* **5**(4), 1185–1192 (1999).
7. J. G. Fujimoto et al., "Optical coherence tomography: an emerging technology for biomedical imaging and optical biopsy," *Neoplasia* **2**(1–2), 9–25 (2000).
8. A. M. Zysk et al., "Optical coherence tomography: a review of clinical development from bench to bedside," *J. Biomed. Opt.* **12**(5), 051403 (2007).
9. S. Boppart et al., "Optical coherence tomography: feasibility for basic research and image-guided surgery of breast cancer," *Breast Cancer Res. Treat.* **84**(2), 85–97 (2004).
10. W. Luo et al., "Optical biopsy of lymph node morphology using optical coherence tomography," *Technol. Cancer Res. Treat.* **4**(5), 539–548 (2005).
11. R. A. McLaughlin et al., "Imaging of human lymph nodes using optical coherence tomography: potential for staging cancer," *Cancer Res.* **70**(7), 2579–2584 (2010).
12. B. J. Vakoc et al., "Cancer imaging by optical coherence tomography: preclinical progress and clinical potential," *Nat. Rev. Cancer* **12**(5), 363–368 (2012).
13. R. A. McLaughlin et al., "Parametric imaging of cancer with optical coherence tomography," *J. Biomed. Opt.* **15**(4), 046029 (2010).
14. J. Strasswimmer et al., "Polarization-sensitive optical coherence tomography of invasive basal cell carcinoma," *J. Biomed. Opt.* **9**(2), 292–298 (2004).
15. Y. Yang et al., "Optical scattering coefficient estimated by optical coherence tomography correlates with collagen content in ovarian tissue," *J. Biomed. Opt.* **16**(9), 090504 (2011).
16. X. Liang et al., "Optical micro-scale mapping of dynamic biomechanical tissue properties," *Opt. Express* **16**(15), 11052–11065 (2008).
17. S. Wang et al., "Noncontact measurement of elasticity for the detection of soft-tissue tumors using phase-sensitive optical coherence tomography combined with a focused air-puff system," *Opt. Lett.* **37**(24), 5184–5186 (2012).
18. E. F. Carbajal et al., "Revealing retroperitoneal liposarcoma morphology using optical coherence tomography," *J. Biomed. Opt.* **16**(2), 020502 (2011).
19. A. M. Zysk and S. A. Boppart, "Computational methods for analysis of human breast tumor tissue in optical coherence tomography images," *J. Biomed. Opt.* **11**(5), 054015 (2006).

20. M. T. Tsai et al., "Effective indicators for diagnosis of oral cancer using optical coherence tomography," *Opt. Express* **16**(20), 15847–15862 (2008).
21. R. K. Manapuram et al., "Estimation of shear wave velocity in gelatin phantoms utilizing PhS-SSOCT," *Laser Phys.* **22**(9), 1–6 (2012).
22. R. K. Manapuram, V. G. R. Manne, and K. V. Larin, "Phase-sensitive swept source optical coherence tomography for imaging and quantifying of microbubbles in clear and scattering media," *J. Appl. Phys.* **105**(10), 102040 (2009).
23. V. V. Tuchin, *Optical Clearing of Tissues, and Blood*, SPIE Press, Bellingham, WA (2006).
24. D. Huang et al., "Optical coherence tomography," *Science* **254**(5035), 1178–1181 (1991).
25. M. J. Kransdorf et al., "Imaging of fatty tumors: distinction of lipoma and well-differentiated liposarcoma," *Radiology* **224**(1), 99–104 (2002).
26. R. A. McLaughlin et al., "Mapping tissue optical attenuation to identify cancer using optical coherence tomography," *Medical Image Computing and Computer-Assisted Intervention—MICCAI 2009*, G.-Z. Yang et al., Eds., pp. 657–664, Springer Berlin Heidelberg, Berlin, Germany (2009).
27. F. A. Tavassoli and P. Devilee, *Pathology & Genetics: Tumours of the Breast and Female Genital Organs*, IARC Press, Lyon, France (2003).
28. W. D. Travis et al., *Pathology & Genetics: Tumours of the Lung, Pleura, Thymus, and Heart*, IARC Press, Lyon, France (2004).
29. D. Lorenser, X. Yang, and D. D. Sampson, "Ultrathin fiber probes with extended depth of focus for optical coherence tomography," *Opt. Lett.* **37**(10), 1616–1618 (2012).
30. D. Lorenser et al., "Ultrathin side-viewing needle probe for optical coherence tomography," *Opt. Lett.* **36**(19), 3894–3896 (2011).